Development of the Motor Periphery is the Rate-Limiting Step in the Ontogeny of the Vestibulo-ocular Reflex

Paige Leary,[1] **Celine Bellegarda**,[1] **Cheryl Quainoo**,[1] **Dena Goldblatt**,[1,2] **Başak Rosti**,[1] **David Schoppik**[1,3,*]
[1] Depts. of Otolaryngology, Neuroscience & Physiology, and the Neuroscience Institute, NYU Grossman School of Medicine
[2] Center for Neural Science, New York University
[2] Lead Contact
[*] Correspondence: schoppik@gmail.com

Sensory deprivation reshapes developing neural circuits, and sensory feedback adjusts the strength of reflexive behaviors throughout life. Sensory development might therefore limit the rate with which behaviors mature, but the complexity of most sensorimotor circuits preclude identifying this fundamental constraint. Here we compared the functional development of components of the vertebrate vestibulo-ocular reflex circuit that stabilizes gaze. We found that vestibular interneuron responses to body tilt sensation developed well before behavioral performance peaked, even without motor neuron-derived feedback. Motor neuron responses developed similarly. Instead, the ontogeny of behavior matched the rate of neuromuscular junction development. When sensation was delayed until after the neuromuscular junction developed, behavioral performance was immediately strong. The matching timecourse and ability to determine behavior establish the development of the neuromuscular junction, and not sensory-derived information, as the rate-limiting process for an ancient and evolutionarily-conserved neural circuit.

In chemistry, the rate-limiting step[1] is a useful simplification to approximate the kinetics of a complex reaction. By analogy, neuroscience might similarly understand the ontogeny of behavior by comparing the rates at which the underlying sensorimotor circuit components develop. Early sensory deprivation profoundly disrupts neural function and associated behaviors in e.g. visual[2], auditory[3], and vestibular[4,5] systems, suggesting that sensory experience/feedback sets the pace of circuit development. Recent therapeutic advances[6–8] underscore the importance of proper development/function of the motor periphery[9]. However, a component's necessity does not confer rate-limiting status. Instead, a rate-limiting component is one whose timecourse of development matches — and determines — the rate of behavioral improvement. Despite recent technological improvements in connectomics for circuit identification[10,11], the complexity and *in utero* development[12] of mammalian circuits complicates measuring rates of development, let alone linking them to behavior.

We studied an archetypal sensorimotor circuit that stabilizes gaze in a simple model vertebrate, the larval zebrafish. The relative simplicity and high conservation of this circuit across vertebrates[13] has made it a powerful model to uncover neural mechanisms of sensorimotor behavior[14]. The vestibulo-ocular reflex circuit consists of sensory afferents that encode motion (e.g. tilts) of the head/body, motor neurons that counter-rotate the eyes with equal and opposite velocity, and interneurons that connect the appropriate sensors to the right motor neurons[15] (Figure 1A). The circuit allows fast, corrective eye movements that, when mature, minimize retinal slip and stabilize gaze. Progressive development of both gaze stabilization behavior[16–19] and vestibulo-ocular reflex circuit components[20–22] is universal across vertebrates. Here we use the transparent, externally-developing larval zebrafish to identify the rate-limiting step in vestibulo-ocular reflex circuit development.

Early ontogeny of gaze stabilization behavior

To determine when behavior matures, we measured the eyes' response to body tilts across early development (Figure 1B). We previously used this approach to define the frequency response of the vestibulo-ocular reflex[23]. Briefly, fish are immobilized with their eye freed and tilted in the pitch axis (nose-up/nose-down) on a rotating platform in complete darkness. Tilt magnitude (15°) and peak velocity (35°/sec) were selected to match the statistics of pitch tilts observed in freely swimming larvae[24]. At and after 5 days post-fertilization (dpf), fish rotated their eyes down following nose-up pitch tilt stimuli (Figure 1C). We parameterized behavioral performance (gain) as the ratio of the peak eye velocity to the peak platform velocity, such that a gain of 1 would fully compensate for retinal slip. Gain improved with age from 3–9 dpf (p_{ANOVA} = 1.01e-9, Figure 1D), reaching gains ~1 and not changing between 9–15 dpf ($p_{post\text{-}hoc}$ = 0.95). These data indicate that behavior improves gradually over the first week of life, and performance plateaus at ~9 dpf.

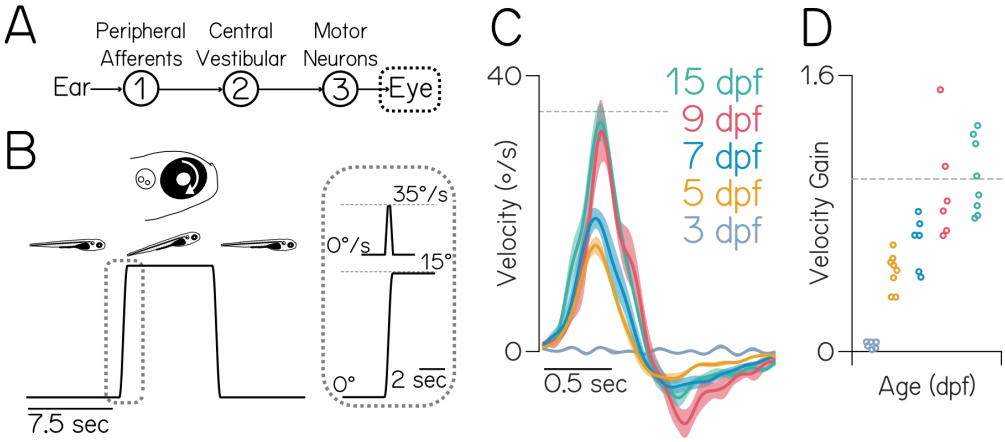

Figure 1: Gaze stabilization matures by 9 days post-fertilization (dpf). (A) Diagram of the gaze stabilization circuit. **(B)** Fish were rotated +15° (nose-up), held for 7.5 sec, then returned. The right eye rotates clockwise, or "down," in response. Gray dotted box shows the trapezoidal velocity profile and angle of the tilt. **(C)** Average eye velocity ±SEM at 3, 5, 7, 9, and 15 dpf (N = 6, 8, 6, 6, 8 fish). **(D)** Gain (peak eye velocity / 35°/sec) for each fish. Gains are significantly different between 3–5 dpf ($p_{post\text{-}hoc}$ = 0.0021), 3–7 dpf ($p_{post\text{-}hoc}$ = 6.51e-5), and 3–9 dpf ($p_{post\text{-}hoc}$ = 4.57e-8), but not 9–15 dpf ($p_{post\text{-}hoc}$ = 0.95). Horizontal line at gain = 1.

Vestibular neuron responses plateau well before behavioral performance peaks, with or without extraocular motor neurons. Vestibular interneuron responses report tilt sensation (Figure 2A). If the development of interneuron responses tracks behavioral improvement, then the rate-limiting process would occur in interneurons or at the sensory periphery. If instead, interneuron development precedes behavior, then the rate-limiting process must occur downstream. To measure the development of vestibular responses to body tilts, we needed to record neural activity at eccentric body postures (Figure 2B), a challenge for conventional imaging with stationary microscopes. We used Tilt In Place Microscopy (TIPM)[25] to avoid rotating the microscope. Instead, TIPM returns fish from an eccentric orientation to the imaging plane faster (~5 msec) than the decay constant of the calcium indicator (GCaMP6s)[26]; the activity observed reflects the decay of the neuron's response when tilted. Neurons in the tangential vestibular nucleus that project to extraocular motor nuclei nIII/nIV are indispensable for the vestibulo-ocular reflex[23,27]. They respond exclusively to either nose-up or nose-down tilts[28], and, when activated optogenetically, they induce torsional eye rotations[27]. We performed longitudinal TIPM (±25°) in these neurons to determine when their responses plateau. We found that vestibular neuron response strength increases dramatically between 3–5 ($p_{t\text{-}test}$ = 1.2e-3, n=22 neurons/N=7 fish) but not between 5–7 or 7–9 dpf ($p_{t\text{-}test}$ = 0.067, n=21/N=7, Figures 2C to 2E).

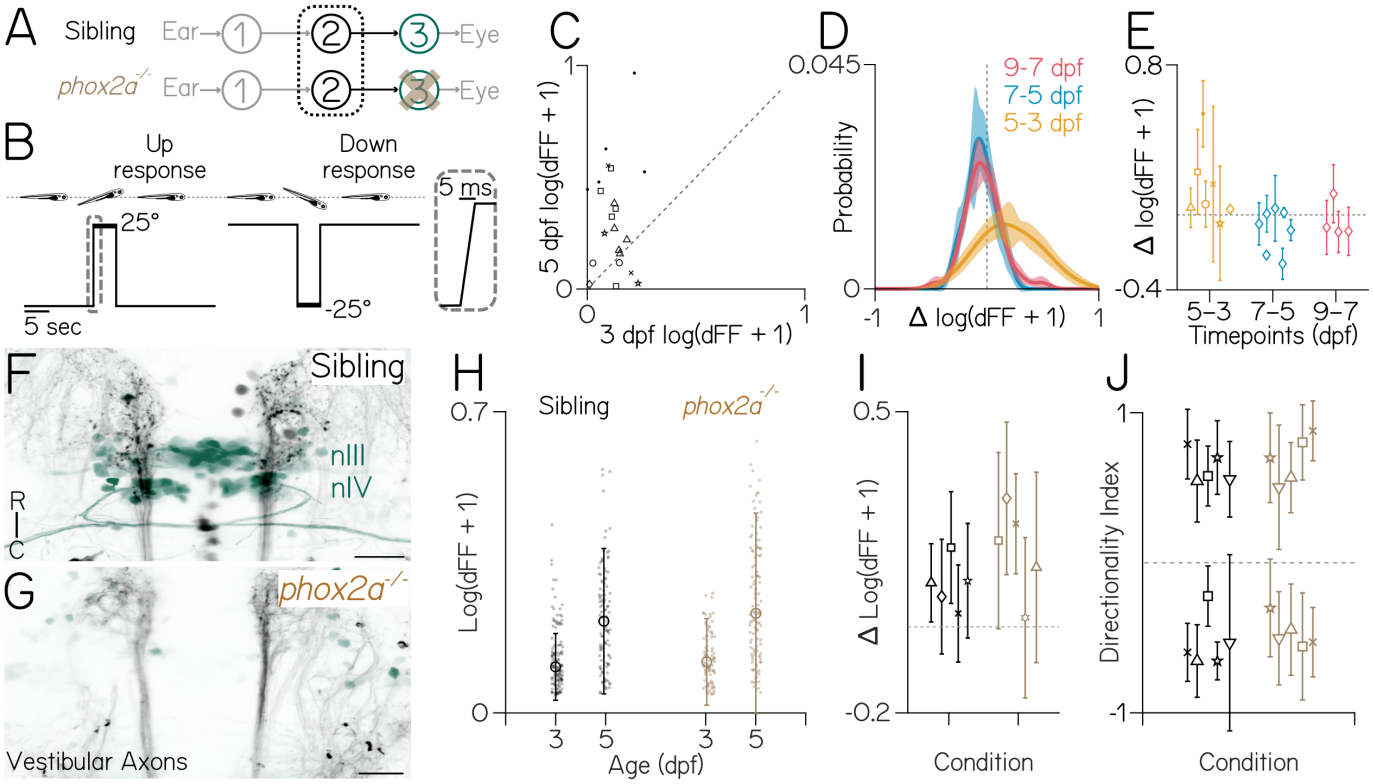

Figure 2: Central vestibular neuron responses also plateau between 3–5 dpf, with or without motor neurons. (A) Diagram of the gaze stabilization circuit, focused on vestibular neurons in fish with and without motor neurons (*phox2a*). **(B)** Vestibular neurons (dotted circles) tracked from 3–7 dpf. Scale bar = 5µm. **(C)** Responses (dFF) to 25° nose-up steps are stronger at 5 dpf than 3 ($p_{t\text{-}test}$ = 1.2e-3). Dashed unity line. **(D)** Distribution ± bootstrapped SD of pairwise differences of individual neurons between days (5-3, 7-5, 9-7 dpf) in response to 25° steps. **(E)** Data from Figure 2D, plotted as the median pairwise difference ±IQR for neurons from each individual fish (N=7,7,4). 5–7 and 7–9 are not different from zero ($p_{t\text{-}test}$ = 0.067 and 0.22). Dashed line at 0. **(F–G)** Axons of central vestibular nuclei (black) to motor neurons in nIII/nIV (green) in a 3 dpf sibling and *phox2a* mutant. Scale bar: 25µm. **(H)** Responses (dots) to 19° pitch tilts in their preferred direction at 3 and 5 dpf. Median ± IQR overlaid. Response changes between 3–5 dpf are significantly different for both siblings and mutants (p_{ANOVA} = 0), with no interaction between age and genotype (p_{ANOVA} = 0.053). **(I)** Data from Figure 2H, plotted as the median pairwise difference ±IQR for paired neurons from each individual fish (n=113 neurons/N=5 siblings, n=116/N=5 *phox2a* mutants). Average response increased between 3–5 dpf with no effect of genotype on this increase (p_{ANOVA} = 5.03e-9 for age effect, p_{ANOVA} = 0.068 for interactions of age and genotype). Dashed line at 0. **(J)** Directionality indices of vestibular neurons at 5 dpf are comparable between *phox2a* null mutants (N=5; n=102) and siblings (N=5,n=112 neurons), plotted as the median ± IQR for each fish ($p_{K\text{-}S\ test}$ = 0.66).

In mature vertebrates, visual feedback signals that follow eye rotations are used to tune the vestibulo-ocular reflex[29]. To determine if eye movement-dependent feedback influences the maturation of vestibular neuron responses, we adopted a loss-of-function approach. We performed TIPM to measure vestibular neuron responses on a *phox2a* mutant background[30] that fails to develop nIII/nIV extraocular motor neurons (Figures 2A, 2F and 2G). Following ±19° tilts, responses of individual neurons (Figure 2H) increased between 3–5 dpf for both sibling fish and mutants (p_{ANOVA} = 1.95e-26, age x genotype p_{ANOVA} = 0.053; 3 dpf: n=137 neurons over N=5 siblings, n=88/N=5 mutants; 5 dpf ; 5 dpf: n=113/N=5 siblings, n=116/N=5 mutants). Across fish (Figure 2I), the average response of paired (tracked) neurons increased between 3–5 dpf (p_{ANOVA} = 0) with no effect of genotype (p_{ANOVA} = 0.069). Finally, to evaluate the development of peripheral vestibular inputs, we examined directional selectivity at 5 dpf. Consistent with a previous report[28], the ratio of nose-up and nose-down sensitive (directionality index values <|0.1|) neurons was nearly even, with no difference between genotype ($p_{K\text{-}S\ test}$ = 0.66; 51.9±6% nose-up, 48±6% nose-down, n=118 neurons over N=5 siblings; 48.1±13% nose-up stimuli, 51.8±13% nose-down, n=117/N=5 *phox2a* mutants) (Figure 2J). These results establish that, even without motor neurons, vestibular neuron responses develop early relative to behavior. Consequentially, the rate-limiting process for behavioral maturation must happen downstream of central vestibular interneurons.

Extraocular motor neuron responses develop between 3–5 dpf

As the last central node in a feed-forward reflex, extraocular motor neuron activity reports the output of all sensory inputs from the entire circuit (Figure 3A). Consequentially, if the development of motor neuron responses reaches a plateau earlier than behavioral im-

provement, the rate-limiting developmental process must occur downstream. We repeated longitudinal TIPM (±25°) in these motor neurons to determine when their responses plateau. However, as the calcium responses of these neurons have not been evaluated in response to body tilts, we first characterized the tuning and sensitivity properties of these neurons to a gradient of stimulus steps (Figure 3B). As expected, superior oblique neurons at 5 dpf responded unidirectionally to nose-up body tilts (Figure 3C) and not to nose-down body tilts (Figure 3D). Motor neuron activity at 5 dpf varied as a function of nose-up tilt eccentricity (n=22/32 neurons with slope > 0, p < 0.05, Figure 3E).

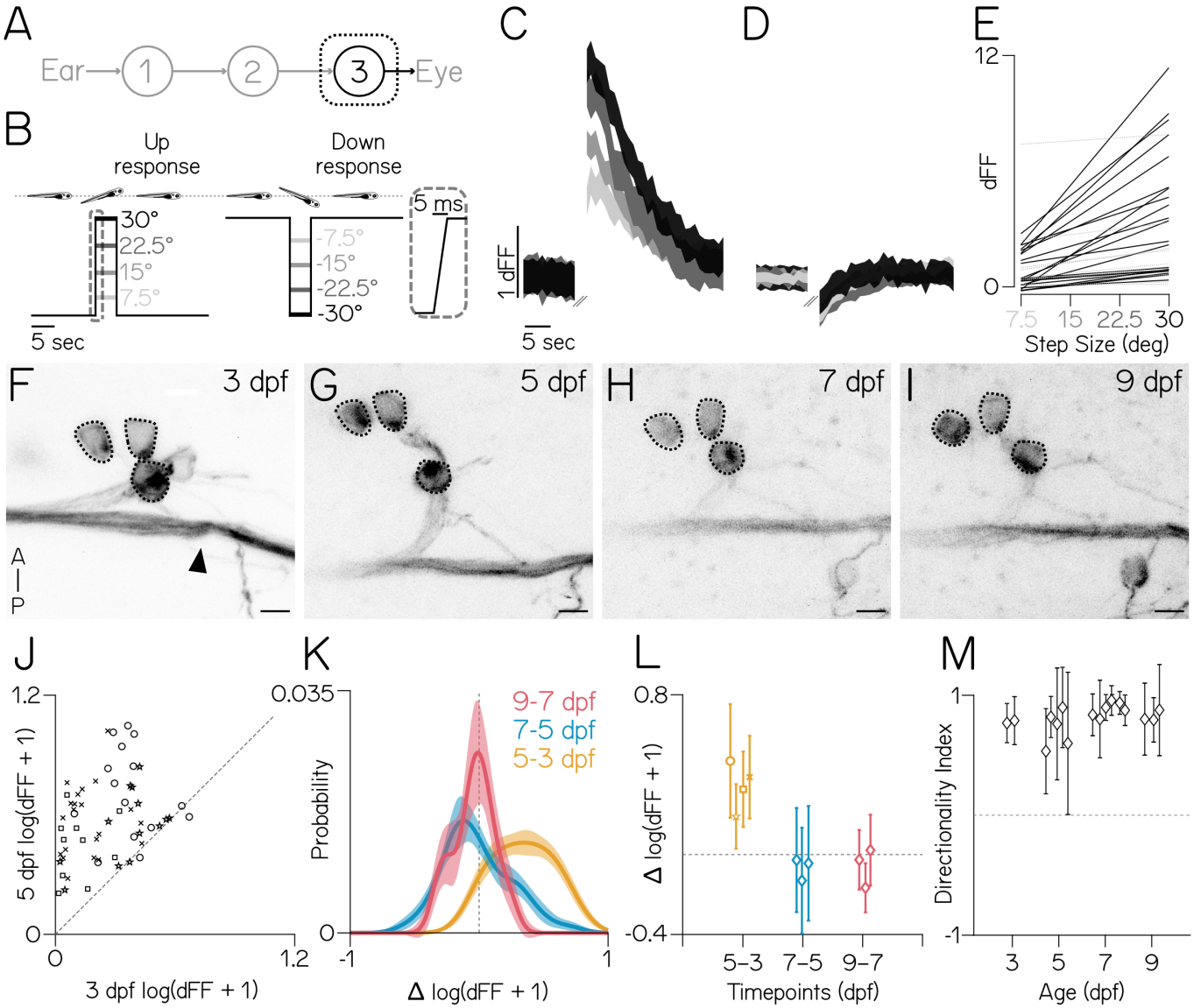

Figure 3: Superior oblique motor neuron responses plateau between 3–5 dpf. **(A)** Diagram of the gaze stabilization circuit, focused on motor neurons. **(B)** A pitch-tilt stimulus trial with a 15 sec baseline, a rapid step (inset, 30° step), a 5 sec eccentric hold, and a rapid return for imaging. **(C–D)** Mean ± SD of responses (dFF) to nose-up (B) and nose-down (C) pitch steps from a single superior oblique extraocular motor neuron at 5 dpf (n=3–5). Pitch amplitude (grayscale) as in Figure 3B. **(E)** Best-fit lines of responses (dFF) from superior oblique motor neurons to nose-up pitch tilts. Black lines have slopes >0 (n=22/32, N=3 fish). **(F–I)** Three superior oblique extraocular motor neurons (dotted circles) and the trochlear nerve (black arrow) tracked from 3–9 dpf. Scale bar = 5μm. **(J)** Responses (dFF) to 25° nose-up steps are greater at 5 dpf than 3 dpf ($p_{t\text{-}test}$ = 1.31e-16). Dashed unity line. **(K)** Distribution ± bootstrapped SD of pairwise differences of individual neurons between days (5-3, 7-5, 9-7 dpf) in response to 25° nose-up steps. **(L)** Data from Figure 3K, plotted as the median pairwise difference for neurons from each individual fish (N=4,3,3). 5–7 and 7–9 are not different from zero ($p_{t\text{-}test}$ = 0.75, 0.23). Dashed line at 0. **(M)** Median ± IQR directionality index to ±25° steps do not change with age $p_{K\text{-}W}$ = 0.09), dashed line at 0. +1 is selective for nose-up, -1 nose-down.

To measure how tilt responses developed, we recorded calcium signals from a transgenic line with sparse expression in superior oblique motor neurons (Figure S1). Motor neuron somata were stably positioned within nIV (Figures 3F to 3I), allowing reliable identification of the same neurons over two-day increments: 3–5 dpf, 5–7 dpf, and 7–9 dpf. To match the pulling direction of the muscle, superior oblique motor neurons should respond predominantly to nose-up tilts. Almost every neuron had a stronger response to 25° nose-up body tilts at 5 dpf compared to 3 ($p_{t\text{-}test}$ = 1.31e-16, n=59 pairs over N=4 fish, Figure 3J). Unlike central vestibular neurons, the distributions of differences varied between 5–7 and 7–9 ($p_{K\text{-}S}$ = 1.9e-16 Figure 3K). Importantly, when evaluated across fish, the average response did not change between 5–7 ($p_{t\text{-}test}$ 0.75, n=45/N=3) or 7–9 ($p_{t\text{-}test}$ = 0.23, n=23/N=3, Figure 3L). We gathered another dataset with 19° nose-up and nose-down steps to evaluate the development of directional selectivity (Methods). We saw no changes across time ($p_{K\text{-}W}$=0.09, 3 dpf: n=16 neurons over N=2 fish; 5 dpf: n=32/N=5; 7 dpf: n=60/N=7; 9 dpf: n=30/N=3, Figure 3M). Since extraocular motor neuron response strength and directional selectivity appear to plateau by 5 dpf — well before behavior — we

conclude that the rate-limiting step for behavioral development is downstream of motor neurons.

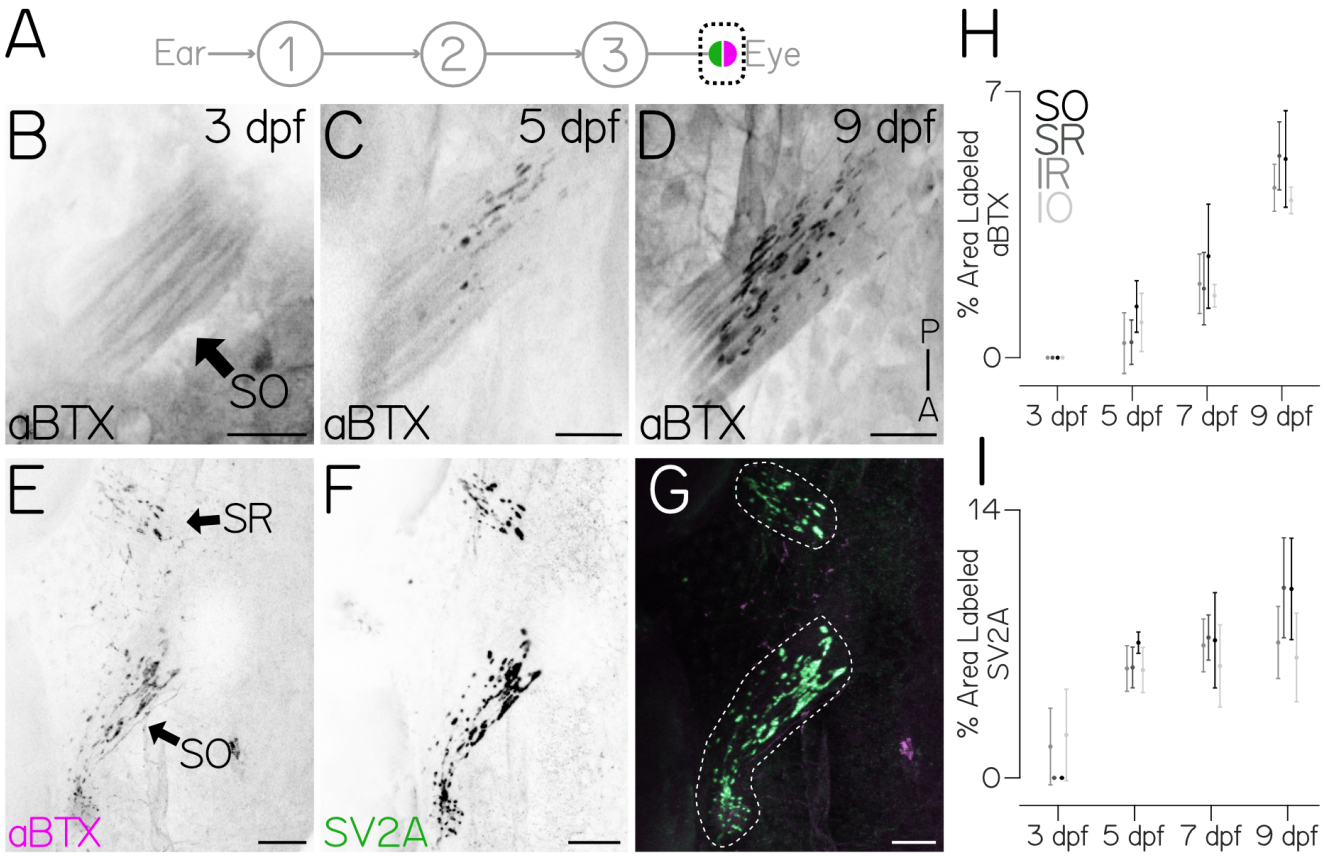

Figure 4: The timecourse of neuromuscular junction development matches behavioral ontogeny.
(A) Diagram of the gaze stabilization circuit. Pre- (green) and postsynaptic (magenta) components of the neuromuscular junction. **(B-D)** Dorsal projection of the superior oblique muscle (black arrow) at 3 (B) 5 (C) and 9 (D) dpf labeled with fluorescent (α-BTX). Scale bar = 20µm **(E-G)** Comparison of superior oblique (SO, arrow) and superior rectus (SR, arrow) pre- (SV2A, green) and postsynaptic (α-BTX, magenta) label at 8 dpf. Dotted line in (G) denotes muscle bound used for quantification. SO muscle: 6.59% α-BTX and 15.03% SV2A. SR muscle: 4.98% α-BTX and 9.33% SV2A. Scale bar = 20µm. **(H)** Postsynaptic α-BTX label in SO, SR, inferior rectus (IR) and inferior oblique (IO) muscles increases with time. Dots are the mean ± SD area labeled. For all muscle types, labeling increased across time (p_{ANOVA} = 0). **(I)** Presynaptic SV2A staining in SO,SR,IR,IO. Dots are the mean ± SD area labeled. For all muscle types, labeling increased across time (p_{ANOVA} = 0.0001). Labeling significantly increased between 3–5 dpf ($p_{post\text{-}hoc}$ = 1.58e-3), but not following 5 dpf (5–7 $p_{post\text{-}hoc}$ = 0.828, 7–9 $p_{post\text{-}hoc}$ = 0.418).

The developmental timecourse of the postsynaptic neuromuscular junction matches the ontogeny of behavior

To evaluate development downstream of motor neurons, we focused on the extraocular neuromuscular junction (Figure 4A). We labeled postsynaptic acetylcholine receptors with fluorescently-conjugated alpha-bungarotoxin (α-BTX, Figures 4B to 4D) and presynaptic vesicles with an SV2A antibody[31] (Figures 4E to 4G). We targeted all four eye muscles used for vertical/torsional gaze stabilization: superior oblique (SO), superior rectus (SR), inferior oblique (IO), inferior rectus (IR) in 3–9 dpf fish. Over time, the fraction of each muscle labelled with α-BTX increased with a timecourse comparable to behavioral improvement (p_{ANOVA} = 0) (SO, n=93 muscles over N=54 fish; SR n=42/N=25; IR n=37/N=24; IO n=31/N=22 Figure 4H). In contrast, SV2A labeling appeared earlier and developed more rapidly. SV2A labeling significantly increased between 3–5 dpf ($p_{post\text{-}hoc}$ = 1.58e-3), but did not change afterwards: ($p_{post\text{-}hoc}$ > 0.13 for 5–7,5–9,7–9, SO, n=24/N=12; SR n=23/N=12; IR n=23/N=12; IO n=23/N=12 Figure 4I). Larval zebrafish eye muscles assume their adult configuration by 3 dpf, with both thick and thin myofibrils by 4 dpf[32], allowing the eye to assume static orientations up to ±30° [23], and a mature optokinetic response (<0.5Hz) by 6 dpf[33]. To determine if the eyes' velocity was constrained by the properties of the muscle, we measured eye movements at 5 dpf following unnaturally rapid tilts (90°/sec, 600°/sec^2 instead of 35°/sec, 150°/sec^2, Figure S2A). We found that although gaze stabilization behavior is far from mature, and the α-BTX signal has just begun to emerge, the eye could rotate faster ($p_{t\text{-}test}$ = 0.016, Figures S2B and S2C). Together these findings implicate the development of the neuromuscular junction as the rate-limiting step for behavioral maturation.

The state of the neuromuscular junction determines vestibulo-ocular reflex behavior

If sensory experience sets the rate of behavioral development, then transient loss of vestibular sensation should delay improvements to gaze stabilization. On restoration, vestibulo-ocular reflex performance should progressively increase. Notably, such a delay would allow the neuromuscular junction to develop. If, instead of sensory experience, the state of the neuromuscular junction determines behavioral performance, then on restoration of vestibular sensation, behavior should be immediately comparable between delayed and non-delayed larvae. Notably, the vestibulo-ocular reflex in congenitally blind fish is mature and indistinguishable from age-matched wild-type siblings (Figure S3), arguing against a role for visual feedback. We investigated the emergence of the vestibulo-ocular reflex in a mutant line (*otogelin*) that, in some cases, is transiently insensitive to body tilts. Under normal conditions[28], larval zebrafish rely exclusively on the utricle to sense body tilts[34], which uses an inertial difference between an otolith and hair cells embedded in a gelatinous macula to transduce linear acceleration. Initial calcification of the utricular otolith normally occurs between 18-24 hpf[35]. The

majority of *otogelin* mutants do not generate a utricular otolith and, in the dark, are tilt-blind[36]. A small fraction of *otogelin* mutants show delayed generation of the utricular otolith, which appears over a 24 hr period around two weeks of age (Figures 5B and 5C), at which point postural behaviors resume[37]. We reasoned that, if development of the neuromuscular junction is rate-limiting, then *otogelin* mutants should show comparable behavior to siblings as soon as the utricle becomes functional.

We first confirmed that the neuromuscular junction developed normally in *otogelin* mutants; we observed strong α-BTX labeling at 8 dpf in both siblings and mutants in all four muscles (Figure 5D). Next, we raised and screened >2000 *otogelin* mutants daily to identify 5 fish with nascent bilateral utricular otoliths between 11–16 dpf (Methods). Eye movements were measured following body tilts (Figure 1B) on the day after identification, when the otolith had reached normal size. Performance was statistically indistinguishable between siblings (N=6) and mutants (N=5) with newly generated otoliths ($p_{post\text{-}hoc}$ = 0.66, Figures 5E and 5F). In contrast, 11–16 dpf fish that never developed otoliths were profoundly impaired ($p_{post\text{-}hoc}$ = 1.84e-7 sibling vs. no otolith, 6.20e-7 delayed otolith vs. no otolith). We infer from the rapid emergence of functional gaze stabilization in *otogelin* mutants that the vestibulo-ocular reflex circuit can assemble properly even in the absence of tilt sensation, consistent with other reports[37,38]. Taken together, these data show that gaze stabilization is determined, not by sensory experience, but instead by development of the neuromuscular junction.

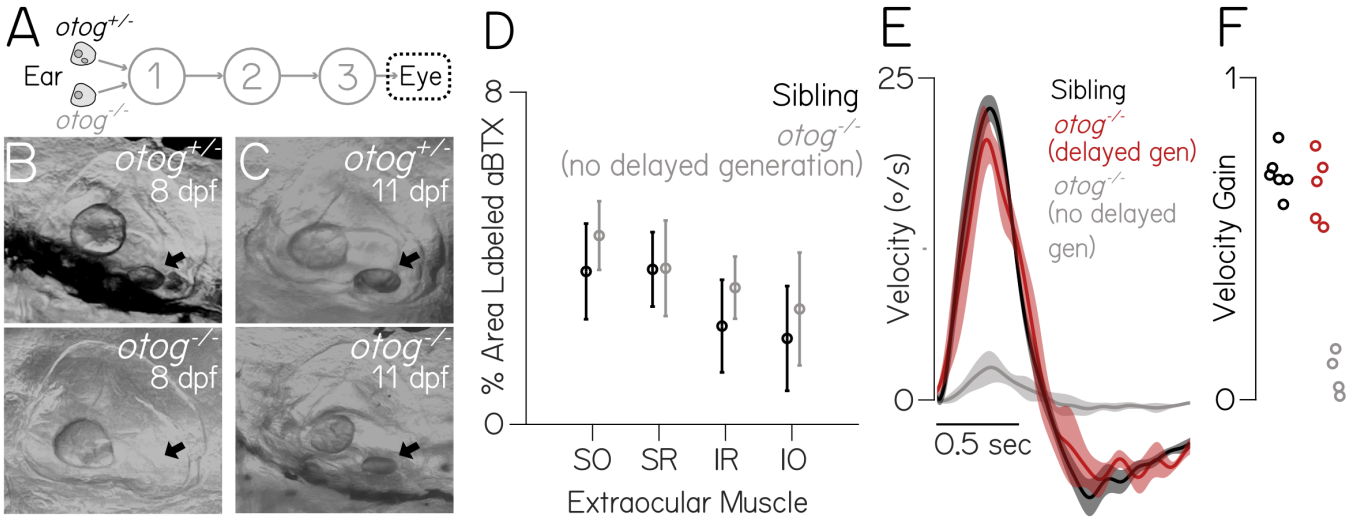

Figure 5: Gaze stabilization behavior emerges rapidly after delayed emergence of tilt sensation

(A) Diagram of the gaze stabilization circuit illustrating *otogelin*$^{-/-}$ phenotype. **(B-C)** Top: *otogelin*$^{+/-}$, utricular otolith visible in ear at 8 (left) and 11 dpf (right, black arrows). Bottom: *otogelin*$^{-/-}$ fish without a utricular otolith at 8, and with at 11 dpf (black arrows). **(D)** Postsynaptic α-BTX label from sibling and *otog*$^{-/-}$ fish SO (N=6,6), SR (N=5,6), IR (N=5,5), IO (N=4,6). **(E)** Average eye velocity traces ±SEM to a nose-up step as in Figure 1B. **(F)** Vestibulo-ocular reflex gain (peak eye / 35°/sec) for each fish (N=6,5,4) in Figure 5E. Gains did not differ between siblings and regenerated *otog*$^{-/-}$ ($p_{post\text{-}hoc}$ = 0.66), unlike *otog*$^{-/-}$ ($p_{post\text{-}hoc}$ = 1.84e-7 and 6.20e-7).

DISCUSSION

We find that, remarkably, both the vestibulo-ocular reflex circuit and behavior can mature without any vestibular input at all. This finding is particularly striking given that gaze stabilization remains plastic throughout life: visual feedback following eye movements is used to adjust the sensitivity of central vestibular neurons to modulate gain[29]. Even when there are no motor neurons to move the eyes, we see that central vestibular neuron responses to tilts are unchanged, underscoring the early dispensability of sensory feedback. In the light, the vestibulo-ocular and optokinetic reflexes work together to stabilize gaze; feedback following optokinetic eye movements might suffice to shape the vestibulo-ocular reflex circuit we studied here. However, such modulation would be inconsistent with our finding that the vestibulo-ocular reflex matures normally in blind fish (Figure S3).Studies of locomotor development over the last century underscore the importance of feedback as animals learn to move properly in their environment[39,40]. Undoubtedly, given the considerable morphological and neurological changes that happen between larval and adult stages, feedback will be similarly important to maintain an excellent vestibulo-ocular reflex. We show that that such plasticity acts on a mature scaffold that can evoke excellent behavior as soon as the neuromuscular junction is sufficiently developed.

By definition, evolutionary adaptations that support earlier/later development of sensorimotor reflex behaviors must manifest with changes to the rate-limiting process. Does the rate of development of the neuromuscular junction limit ontogeny of other behaviors? Early neuromuscular junction development permits developing rodents to make spontaneous limb contractions, or "twitches," that can shape sensory cortical[41] and cerebellar development[42]. Similar twitches[43] precede development of the hindbrain neurons responsible for evoked escape swimming in larval zebrafish[44], the earliest sensorimotor reflex behavior; by inference, the rate-limiting process for escapes is upstream of the motor periphery. Differences in the location of the rate limiting process may reflect selective pressures that differ between precocial (mobile at birth) and altricial (immobile) animals. Empirically, when the pressure is on to stand/run/swim or be eaten, the motor periphery develops much more rapidly to ensure that "the neuromuscular system [is] ready for use when the brain needs it"[45]. We suggest that defining the location of rate-limiting processes will speak to how circuits came to be.

Recent advances in transcriptomics and connectomics[10,11] revealed the elements of and interactions between vertebrate neural circuit nodes. Similar advances transformed longitudinal[46] and circuit-level[47] measurements linking neuronal activity and behavior[48]. In contrast, conceptual frameworks[49] lag behind, relying primarily on classic loss-of-function approaches to establish necessity[50]. Here, motivated by a powerful simplification in chemistry[1], we discovered the rate-limiting process for the maturation of a vertebrate sensorimotor behavior. Our approach moves beyond "necessity," linking neural circuit development to behavioral performance.

MATERIALS AND METHODS

Fish Care

All procedures involving zebrafish larvae (*Danio rerio*) were approved by the New York University Langone School of Medicine Institutional Animal Care and Use Committee (IACUC). Fertilized eggs were collected and maintained at 28.5°C on a standard 14h light/10 h dark cycle. Before 5 dpf, larvae were maintained at densities of 20–50 larvae/10-cm-diameter Petri dish, filled with 25–40 mL of E3 with 0.5 ppm methylene blue. After 5 dpf, larvae were maintained at densities under 20 larvae/Petri dish and were fed cultured rotifers (Reed Mariculture) daily.

Transgenic lines

Functional imaging and confocal experiments were conducted on the *mitfa*$^{-/-}$ background to remove pigment. Two-photon calcium imaging experiments were performed on the *Tg(isl1:GAL4)*^{fh452};*Tg(14xUAS:GCaMP6s)* background[51,52]. Confocal imaging experiments used larvae of Tg(isl1:GFP) background[53]. α-bungarotoxin and SV2A labeling experiments used larvae from the *roy* (*mpv17*$^{a9/a9}$) background[54] to eliminate autofluorescence from iridiphores of the eye. Vestibular projection neuron functional imaging was performed using the *Tg(-6.7Tru.Hctr2:GAL4-VP16)* line[55]. Motor neuron loss-of-function experiments were performed on larvae from F3 or older generations of *phox2a* mutants[30], screened on the *Tg(isl1:GFP)* background for the presence or absence of fluorescence in nIII/nIV. *otogelin* mutants were rks$^{vo66/vo66}$[36]. Blind fish were from the *lakritz* (*atoh7*$^{th241/241}$) background that does not develop retinal ganglion cells[56]. *Tg(14xUAS-E1B:KillerRed)*[57] was used for visualization. All larvae used were selected for brightness of fluorescence relative to siblings. Mendelian ratios were observed, supporting that selected larvae were homozygous for a given allele.

Confocal Imaging

Larvae were anesthetized in 0.2 mg/mL ethyl-3-aminobenzoic acid ethyl ester (MESAB, Sigma-Aldrich E10521, St. Louis, MO) prior to imaging. Larvae were mounted dorsal side-up (axial view) in 2% low-melting point agarose (Thermo Fisher Scientific 16520) in E3. Images were collected on a Zeiss LSM800 confocal microscope with a 20x water-immersion objective (Zeiss W Plan-Apochromat 20x/1.0). Anatomical stacks of nIII/nIV spanned approximately 100µm in depth, sampled every two microns. Image stacks were analyzed using Fiji/ImageJ[58].

Tilt In Place Microscopy (TIPM)

TIPM is an imaging technique to measure neural responses to body tilts by rapidly rotating larvae (peak angular velocity, <3,000°/s) and peak acceleration (>1e7°/s^2)[25]. Briefly, larvae aged 3, 5, 7, or 9 dpf were mounted dorsal-up in 2% low-melt agarose in E3 in the center of the mirror of a large beam diameter single-axis scanning galvanometer system (ThorLabs GVS011, 10 mm 1D, 40° range). A single trial consisted of of a 15 sec pre-stimulus baseline, a rapid (textasciitilde5 msec) eccentric step, 5 sec at the eccentric tilt, a rapid (~5 msec) return to baseline, and a 20 sec period at the horizontal. Experiments mapping the sensitivity of motor neurons consisted of 4–5 repeats of 7.5°, 15°, 22.5°, or 30° steps, order randomized, lasting ~2 hrs/fish. To use the full range of the galvonometer, sensitivity-mapping stimuli were presented in a single pitch direction (nose-up or nose-down) at a time; direction order was randomized. Longitudinal experiments were performed similarly, using a single 25° step presented 4–5 times, lasting ~1 hr/fish. All experiments took place in complete darkness.

All stimuli were presented while imaging with a two-photon microscope (ThorLabs Bergamo) using a 20x water immersion objective (Olympus XLUMPLFLN20xW 20x/1.0). Illumination consisted of a pulsed infrared laser (Spectra-Physics MaiTai HP) at 920 nm using 6.1–18.8 mW of power, measured at the sample using a power meter (ThorLabs S130C).

For motor neuron imaging, volumes were centered over nIV in both hemisphere, with the trochlear nerve visible in each stack. Each volume consisted of 4–6 planes spanning 70µm in the dorso-ventral axis. Because expression was sparse and variegated in the *Tg(isl1:GAL4)*; *Tg(UAS:GCaMP6s* line, the imaging window was optimized to cover all labelled nIV cells for each fish. Imaging was performed at ~3 volumes/sec (~26 frames/sec, ~74–150 x 50µm frame size, and 1µsec pixel dwell time).

For imaging of vestibular neurons in the tangential nucleus in *phox2a*$^{-/-}$ fish and siblings, experiments were performed at 3 and 5 dpf. Larvae were sorted at 2 dpf into *phox2a*$^{-/-}$ and sibling controls (non-phenotypic) based on the absence or presence of labeled extraocular motor neurons using the *isl1:GFP* transgene. Imaging volumes were centered over the tangential nucleus[28], one hemisphere at a time. Each volume consisted of 4-5 planes spanning 30µm in the dorso-ventral axis. Imaging was performed at ~3 volumes/second (~20frames/second, ~100x60µm frame size, and 1µs pixel dwell time).

Analysis of TIPM data

Volumes were pre-processed using Fiji/ImageJ[58]. Each volume was motion-corrected to account for any slight shifts in the X or Y axes across multiple trials[59]. Polygonal regions of interest (ROI) were drawn manually around all neuron somata visible in an average intensity projection. All neurons were included for analysis.

All subsequent analyses were performed using Matlab R2020b (MathWorks, Natick, MA, USA). Raw fluorescence traces from ROIs were extracted and, when imaging zoom had varied, normalized by ROI size to compensate for different pixel sizes. A neuron's response was defined as the normalized change in fluorescence (dFF). dFF was calculated by taking the peak during the first second on return to horizontal, subtracting the baseline, and dividing by the baseline. Baseline fluoresence was defined as the average value over the first 10 frames at the beginning of each trial. To quantify the strength of directional tuning, a directionality index was calculated for each neuron. The directionality index (from -1 to 1) is defined as the difference in up/down dFF normalized by their sum. A neuron was defined as "tuned" if the absolute value of the directionality index was >0.1. Data are presented as log(dFF+1) to better visualize the full range of responses.

Tracking Individual Neurons Across Time

Motor neurons and tangential nucleus neurons were manually tracked across three time points: 3–5 dpf, 5–7 dpf, and 7–9 dpf. TIPM data was used to define the soma position and, for motor neurons, the distance from the trochlear nerve. To ensure reliability, neurons across time were tracked independently by two separate experimenters (P.L. and either C.B. or C.Q); only neurons where experimenters agreed were included. After 5 dpf, somata remained stationary, facilitating tracking. The majority of neurons recorded following 5 dpf were identifiable at the second time points (64.4±19.4% between 5 and 7 dpf, 53.7±15.2% between 7 and 9 dpf). Before 5 dpf, some soma shifting was observed (typically in a caudal-to-rostral direction for motor neurons), and therefore an additional anatomy stack was taken at 4 dpf to more facilitate tracking neurons across time. The yield of confidently tracked neurons between 3 and 5 dpf was 59.7±19.9%.

Whole-Mount Immunohistochemistry and Synaptic Labeling

Larvae were fixed and permeabilized as described in[60]. Briefly, fish were anesthetized in 0.2 mg/mL MESAB then fixed in 4% paraformaldehyde overnight at 4°C. Following overnight fixation, fish were washed in and stored in 100% methanol at -20°C. On the day of staining, fish were rehydrated in decreasing concentrations of methanol (75%, 50%, 25%) and washed in phosphate buffered saline with 0.1% Tween (PBST). Larvae labeled with the presynaptic vesicle antibody SV2A (DSHB SV2-s, 52µg/mL, RRID: AB_2315387) were prepared as described elsewhere[61]. Briefly, following rehydration, larvae were further permeabilized in PBS with 0.5% Triton and incubated in a blocking solution (1% BSA in PBT, 2.5% DMSO, and 5% HINGS). Larvae were then incubated for four nights in 3µg/µL of SV2A primary antibody at 4°C. Secondary antibody incubation was performed overnight at 1:1000 concentration in AlexaFluor 488nm goat anti-mouse (Invitrogen, A28175, RRID: AB_2535719). Alpha-bungarotoxin (αBTX) labeling was performed following a similar method as described previously[62]. Following fixation and rehydration, larvae were incubated in 50µg /µL αBTX conjugated to AlexaFluor 647nm (ThermoFisher, B35450) for 45 minutes at room temperature in the dark. Fixed larvae double-labeled with SV2A and αBTX followed the SV2A antibody protocol as described above; following secondary antibody incubation and PBST wash, larvae were incubated in 50µg /µL BTX for 45 minutes prior to confocal imaging. Prior to labeling, all larvae were washed in PBST in the dark and mounted dorsal-side up in 2% low-melting point agarose (Thermo Fisher Scientific 16520) in E3 prior to imaging.

Neuromuscular Junction Imaging and Quantification

Stacks of extraocular muscle were collected on a confocal microscope (Zeiss LSM800) with a 20x water-immersion objective (Zeiss W Plan-Apochromat 20x/1.0). The imaging window was centered on a single hemisphere over one eye at a time, 200–250 x 200–250 µm frame size. Stacks were collected through the full dorso-ventral extent of the muscle (~30µm) with an imaging interval of 2µm. For all extraocular muscles, the imaging window was centered over one eye at a time with either both superior oblique and rectus (dorsal-up orientation) or both inferior oblique and rectus muscles (ventral-up orientation) in view.

Quantification of αBTX labeling in extraocular muscle was performed in FIJI/ImageJ[58]. Maximum intensity projections of single-color grayscale stacks were made with the full muscle in view. Polygonal ROIs were drawn around the entirety of the extraocular muscle. Images were thresholded by intensity to differentiate the brightest signal (postsynaptic neuromuscular junction label) from the weakest signal (muscle fiber). Thresholding was repeated by two investigators independently to ensure consistency. Thresholded images were then binarized. "% Area Labeled" is defined as the fraction of suprathreshold pixels within each muscle's ROI. Next, average particle sizes were computed with a set size of 1-infinity and converted to µm.

Behavior Experiments & Analysis

Torsional eye rotations were measured in response to step tilts delivered using an apparatus similar in design to[23]. All experiments took place in complete darkness. Larval fish were immobilized completely in 2% low-melting temperature agarose, and the left eye freed. The agarose was then pinned (0.1mm stainless minutien pins, FST) to a ~5mm^2 piece of Sylgard 184 (Dow Corning) which was itself pinned to Sylgard 184 at the bottom of a 10mm^2 optical glass cuvette (Azzota, via Amazon). Within age groups, body length was confirmed to be consistent to ensure matched developmental maturation[63,64]. The cuvette was filled with ~1mL of E3 and placed in a custom holder on a 5-axis (X,Y,Z,pitch,roll) manipulator (ThorLabs MT3 and GN2). The fish was aligned with the optical axes of two orthogonally placed cameras such that both the left utricle and two eyes were level with the horizon (front camera) and centered about the axis of rotation. The eye-monitoring camera (Guppy Pro 2 F-031, Allied Vision Technologies) used a 5x objective (Olympus MPLN, 0.1 NA) and custom image-forming optics to create a 100x100 pixel image of the left eye of the fish (6 µm/pixel), acquired at 200Hz. The image was processed on-line by custom pattern matching software to derive an estimate of torsional angle (LabView 2014, National Instruments), and data was analyzed using custom MATLAB scripts (Mathworks, Natick MA).

A stepper motor (Oriental Motors AR98MA-N5-3) was used to rotate the platform holding the cameras and fish. Microstep commands (0.0072°) were delivered with varying intervals to enable smooth speed control according to the algorithm in[65]. An experiment consisted of 50 cycles of four steps each. Steps were $\pm 15°$ towards and away from the horizon. Each step followed a trapezoidal velocity profile peaking at either 35°/sec, peak acceleration 150°/sec^2 (normal) or 90°/sec (fast controls), peak acceleration 600°/sec^2. The platform velocity and acceleration were measured using integrated circuits (IDG500, Invensense and ADXL335, Analog Devices) mounted together on a breakout board (Sparkfun SEN-09268).

The eye's response across the experiment was first centered to remove any offset introduced by the pattern-matching algorithm. Data were then interpolated with a cubic spline to correct for occasional transient slowdowns (i.e. missed frames). The eye's velocity was estimated by differentiating the position trace; high-frequency noise was minimized using a 4-pole low-pass Butterworth filter (cutoff = 3Hz). Each step response was evaluated manually; trials with rapid deviations in eye position indicative of horizontal saccades or gross failure of the pattern-matching algorithm were excluded from analysis. The response to each step for a given fish was defined as the mean across all responses to that step across cycles. The gain was estimated by measuring the peak eye velocity occurring over the first second after the start of the step.

Statistics

Parametric data were tested with Student's t-test, paired t-tests for longitudinal data (i.e. comparing the same neuron), 1- and 2-way ANOVA with post-hoc comparisons, repeated measures design used for longitudinal data. Non-parametric data were tested using Kruskall-Wallis (K-W) tests. When appropriate, α was Bonferroni corrected for multiple comparisons, with a significance threshold of 0.05. A Kolmogorov-Smirnov (K-S) test was used to compare distributions of directionality indices. Population standard deviations were generated by bootstrapping (i.e resampling with replacement), n=60 repeats. Statistical tests were done on log-transformed data (dFF+1). All tests were repeated on raw data using non-parametric equivalents and the conclusions did not change, with one exception: in Figure 3J the 3–5 dpf differences between populations of neurons in *phox2a*$^{-/-}$ and sibling fish changed from p_{ANOVA} = 0.053 to $p_{K\text{-}W}$ = 0.0032. All tests reported in the text as subscripts; $p_{post\text{-}hoc}$ refers to post-hoc pairwise comparisons after ANOVA/K-W using Tukey's honestly significant difference procedure.

Data & Code Availability

All raw data and analysis code are available at the Open Science Foundation, DOI: 10.17605/OSF.IO/7Z5UP

ACKNOWLEDGMENTS

Research was supported by the National Institute on Deafness and Communication Disorders of the National Institutes of Health under award numbers R01DC017489 and F31DC020910, the National Institute for Neurological Disorders and Stroke of the National Institutes of Health under award number F99NS129179, as well as the National Science Foundation under Graduate Research Fellowship number DGE2041775. The authors would like to thank Cecilia Moens and Martha Bagnall for all the fish, Hannah Gelnaw

for assistance with husbandry, and Katherine Nagel, Jeremy Dasen, Niels Ringstad, Lynne Kiorpes, Michael Long, György Buzsáki, Alexander Schier along with the members of the Schoppik and Nagel labs for their valuable feedback and discussions.

AUTHOR CONTRIBUTIONS

Conceptualization: PL and DS, Methodology: PL, CB, CQ, DG, BR, and DS, Investigation: PL, Visualization: PL, Writing: PL and DS, Editing: PL and DS, Funding Acquisition: PL and DS, Supervision: DS.

AUTHOR COMPETING INTERESTS

The authors declare no competing interests.

REFERENCES

[1] F. F. Blackman. Optima and limiting factors. *Annals of Botany*, os-19(2):281296, April 1905.
[2] David H. Hubel and Torsten N. Wiesel. Effects of monocular deprivation in kittens. *Naunyn-Schmiedebergs Archiv fr Experimentelle Pathologie und Pharmakologie*, 248(6):492497, 1964.
[3] Edward F. Chang and Michael M. Merzenich. Environmental noise retards auditory cortical development. *Science*, 300(5618):498502, April 2003.
[4] Marc Jamon. The development of vestibular system and related functions in mammals: impact of gravity. *Frontiers in Integrative Neuroscience*, 8, 2014.
[5] Christopher T. Goode, Donna L. Maney, Edwin W Rubel, and Albert F. Fuchs. Visual influences on the development and recovery of the vestibuloocular reflex in the chicken. *Journal of Neurophysiology*, 85(3):11191128, March 2001.
[6] Sumimasa Arimura, Takashi Okada, Tohru Tezuka, Tomoko Chiyo, Yuko Kasahara, Toshiro Yoshimura, Masakatsu Motomura, Nobuaki Yoshida, David Beeson, Shinichi Takeda, and Yuji Yamanashi. Dok7 gene therapy benefits mouse models of diseases characterized by defects in the neuromuscular junction. *Science*, 345(6203):15051508, September 2014.
[7] Julien Oury, Wei Zhang, Nadia Leloup, Akiko Koide, Alexis D. Corrado, Gayatri Ketavarapu, Takamitsu Hattori, Shohei Koide, and Steven J. Burden. Mechanism of disease and therapeutic rescue of dok7 congenital myasthenia. *Nature*, 595(7867):404408, June 2021.
[8] Linda K. McLoon, Stephen P. Christiansen, Geoffrey M. Ghose, Vallabh E. Das, and Michael J. Mustari. Improvement of eye alignment in adult strabismic monkeys by sustained igf-1 treatment. *Investigative Opthalmology & Visual Science*, 57(14):6070, November 2016.
[9] Joshua R. Sanes and Jeff W. Lichtman. Development of the vertebrate neuromuscular junction. *Annual Review of Neuroscience*, 22(1):389442, March 1999.
[10] Jingtian Zhou, Zhuzhu Zhang, May Wu, Hanqing Liu, Yan Pang, Anna Bartlett, Zihao Peng, Wubin Ding, Angeline Rivkin, Will N. Lagos, Elora Williams, Cheng-Ta Lee, Paula Assakura Miyazaki, Andrew Aldridge, Qiurui Zeng, J. L. Angelo Salinda, Naomi Claffey, Michelle Liem, Conor Fitzpatrick, Lara Boggeman, Zizhen Yao, Kimberly A. Smith, Bosiljka Tasic, Jordan Altshul, Mia A. Kenworthy, Cynthia Valadon, Joseph R. Nery, Rosa G. Castanon, Neelakshi S. Patne, Minh Vu, Mohammad Rashid, Matthew Jacobs, Tony Ito, Julia Osteen, Nora Emerson, Jasper Lee, Silvia Cho, Jon Rink, Hsiang-Hsuan Huang, António Pinto-Duartec, Bertha Dominguez, Jared B. Smith, Carolyn OConnor, Hongkui Zeng, Shengbo Chen, Kuo-Fen Lee, Eran A. Mukamel, Xin Jin, M. Margarita Behrens, Joseph R. Ecker, and Edward M. Callaway. Brain-wide correspondence of neuronal epigenomics and distant projections. *Nature*, 624(7991):355365, December 2023.
[11] Li Yuan, Xiaoyin Chen, Huiqing Zhan, Henry L. Gilbert, and Anthony M. Zador. Massive multiplexing of spatially resolved single neuron projections with axonal barseq. *bioRxiv*, February 2023.
[12] Moriah E. Thomason. Development of brain networks in utero: Relevance for common neural disorders. *Biological Psychiatry*, 88(1):4050, July 2020.
[13] Hans Straka and Robert Baker. Vestibular blueprint in early vertebrates. *Frontiers in Neural Circuits*, 7, 2013.
[14] Jay M. Goldberg, Victor J. Wilson, Kathleen E. Cullen, Dora E. Angelaki, Dianne M. Broussard, Jean Buttner-Ennever, Kikuro Fukushima, and Lloyd B. Minor. *The Vestibular System: A Sixth Sense*. Oxford University Press, March 2012.
[15] John Szentágothai. The elementary vestibulo-ocular reflex arc. *Journal of Neurophysiology*, 13(6):395407, November 1950.
[16] E. Horn, H. G. Lang, and B. Rayer. The development of the static vestibulo-ocular reflex in the southern clawed toad, xenopus laevis: I. intact animals. *Journal of Comparative Physiology A*, 159(6):869878, 1986.
[17] Bernd Michael Faulstich, Kimberly Ann Onori, and Sascha du Lac. Comparison of plasticity and development of mouse optokinetic and vestibulo-ocular reflexes suggests differential gain control mechanisms. *Vision Research*, 44(28):34193427, December 2004.
[18] Sandra L. Shea. *Eye Movements: Developmental Aspects*, page 239306. Elsevier, 1992.
[19] J.M. Flandrin, J.H. Courjon, and M. Jeannerod. Development of vestibulo-ocular response in the kitten. *Neuroscience Letters*, 12(23):295299, May 1979.
[20] L. Carrascal, J.L. Nieto-Gonzalez, P. Núñez-Abades, and B. Torres. Temporal sequence of changes in electrophysiological properties of oculomotor motoneurons during postnatal development. *Neuroscience*, 140(4):12231237, 2006.
[21] JD Porter and RS Baker. Prenatal morphogenesis of primate extraocular muscle: neuromuscular junction formation and fiber type differentiation. *Investigative ophthalmology & visual science*, 33(3):657–670, 1992.
[22] Mei Shao, June C. Hirsch, and Kenna D. Peusner. Emergence of action potential generation and synaptic transmission in vestibular nucleus neurons. *Journal of Neurophysiology*, 96(3):12151226, September 2006.
[23] Isaac H. Bianco, Leung-Hang Ma, David Schoppik, Drew N. Robson, Michael B. Orger, James C. Beck, Jennifer M. Li, Alexander F. Schier, Florian Engert, and Robert Baker. The tangential nucleus controls a gravito-inertial vestibulo-ocular reflex. *Current Biology*, 22(14):12851295, July 2012.
[24] Yunlu Zhu, Franziska Auer, Hannah Gelnaw, Samantha N. Davis, Kyla R. Hamling, Christina E. May, Hassan Ahamed, Niels Ringstad, Katherine I. Nagel, and David Schoppik. Sampl is a high-throughput solution to study unconstrained vertical behavior in small animals. *Cell Reports*, 42(6):112573, June 2023.
[25] Kyla R. Hamling, Yunlu Zhu, Franziska Auer, and David Schoppik. Tilt in place microscopy: a simple, low-cost solution to image neural responses to body rotations. *The Journal of Neuroscience*, 43(6):936948, December 2022.
[26] Tsai-Wen Chen, Trevor J. Wardill, Yi Sun, Stefan R. Pulver, Sabine L. Renninger, Amy Baohan, Eric R. Schreiter, Rex A. Kerr, Michael B. Orger, Vivek Jayaraman, Loren L. Looger, Karel Svoboda, and Douglas S. Kim. Ultrasensitive fluorescent proteins for imaging neuronal activity. *Nature*, 499(7458):295300, July 2013.
[27] David Schoppik, Isaac H. Bianco, David A. Prober, Adam D. Douglass, Drew N. Robson, Jennifer M.B. Li, Joel S.F. Greenwood, Edward Soucy, Florian Engert, and Alexander F. Schier. Gaze-stabilizing central vestibular neurons project asymmetrically to extraocular motoneuron pools. *The Journal of Neuroscience*, 37(47):1135311365, September 2017.
[28] Dena Goldblatt, Stephanie Huang, Marie R. Greaney, Kyla R. Hamling, Venkatakaushik Voleti, Citlali Perez-Campos, Kripa B. Patel, Wenze Li, Elizabeth M.C. Hillman, Martha W. Bagnall, and David Schoppik. Neuronal birthdate reveals topography in a vestibular brainstem circuit for gaze stabilization. *Current Biology*, 33(7):1265–1281.e7, April 2023.
[29] S Lac, J L Raymond, T J Sejnowski, and S G Lisberger. Learning and memory in the vestibulo-ocular reflex. *Annual Review of Neuroscience*, 18(1):409441, March 1995.
[30] Dena Goldblatt, Baak Rosti, Kyla R. Hamling, Paige Leary, Harsh Panchal, Marlyn Li, Hannah Gelnaw, Stephanie Huang, Cheryl Quainoo, and David Schoppik. Motor neurons are dispensable for the assembly of a sensorimotor circuit for gaze stabilization. *bioRxiv*, January 2024.
[31] K Buckley and R B Kelly. Identification of a transmembrane glycoprotein specific for secretory vesicles of neural and endocrine cells. *The Journal of cell biology*, 100(4):12841294, April 1985.
[32] Stephen S. Easter and Gregory N. Nicola. The development of eye movements in the zebrafish (danio rerio). *Developmental Psychobiology*, 31(4):267276, December 1997.
[33] James C. Beck, Edwin Gilland, David W. Tank, and Robert Baker. Quantifying the ontogeny of optokinetic and vestibuloocular behaviors in zebrafish, medaka, and goldfish. *Journal of Neurophysiology*, 92(6):35463561, December 2004.
[34] Bruce B. Riley and Stephen J. Moorman. Development of utricular otoliths, but not saccular otoliths, is necessary for vestibular function and survival in zebrafish. *Journal of Neurobiology*, 43(4):329337, 2000.
[35] Bruce B. Riley, Chenwei Zhu, Chris Janetopoulos, and Karl J. Aufderheide. A critical period of ear development controlled by distinct populations of ciliated cells in the zebrafish. *Developmental Biology*, 191(2):191201, November 1997.
[36] Tanya T. Whitfield, Michael Granato, Fredericus J. M. van Eeden, Ursula Schach, Michael Brand, Makoto Furutani-Seiki, Pascal Haffter, Matthias Hammerschmidt, Carl-Philipp Heisenberg, Yun-Jin Jiang, Donald A. Kane, Robert N. Kelsh, Mary C. Mullins, Jörg Odenthal, and Christiane Nüsslein-Volhard. Mutations affecting development of the zebrafish inner ear and lateral line. *Development*, 123(1):241254, December 1996.
[37] Richard Roberts, Jeffrey Elsner, and Martha W. Bagnall. Delayed otolith development does not impair vestibular circuit formation in zebrafish. *Journal of the Association for Research in Otolaryngology*, 18(3):415425, March 2017.
[38] Florian Ulrich, Charlotte Grove, Jesus Torres-Vazquez, and Robert Baker. Development of functional hindbrain oculomotor circuitry independent of both vascularization and neuronal activity in larval zebrafish. *Current Neurobiology*, 7, 2016.
[39] Karen E. Adolph, Bennett I. Bertenthal, Steven M. Boker, Eugene C. Goldfield, and Eleanor J. Gibson. Learning in the development of infant locomotion. *Monographs of the Society for Research in Child Development*, 62(3):i, 1997.
[40] Esther Thelen. Motor development as foundation and future of developmental psychology. *International Journal of Behavioral Development*, 24(4):385397, December 2000.
[41] Rustem Khazipov, Anton Sirota, Xavier Leinekugel, Gregory L. Holmes, Yehezkel Ben-Ari, and György Buzsáki. Early motor activity drives spindle bursts in the developing somatosensory cortex. *Nature*, 432(7018):758761, December 2004.
[42] James C. Dooley, Greta Sokoloff, and Mark S. Blumberg. Movements during sleep reveal the developmental emergence of a cerebellar-dependent internal model in motor thalamus. *Current Biology*, 31(24):5501–5511.e5, December 2021.
[43] Louis Saint-Amant and Pierre Drapeau. Time course of the development of motor behaviors in the zebrafish embryo. *Journal of Neurobiology*, 37(4):622632, December 1998.

[44] Rober C. Eaton and Roger D. Farley. Development of the mauthner neurons in embryos and larvae of the zebrafish, brachydanio rerio. *Copeia*, 1973(4):673, December 1973.
[45] D Kernell. The final common pathway in postural controldevelopmental perspective. *Neuroscience & Biobehavioral Reviews*, 22(4):479484, March 1998.
[46] Nicholas A. Steinmetz, Cagatay Aydin, Anna Lebedeva, Michael Okun, Marius Pachitariu, Marius Bauza, Maxime Beau, Jai Bhagat, Claudia Böhm, Martijn Broux, Susu Chen, Jennifer Colonell, Richard J. Gardner, Bill Karsh, Fabian Kloosterman, Dimitar Kostadinov, Carolina Mora-Lopez, John OCallaghan, Junchol Park, Jan Putzeys, Britton Sauerbrei, Rik J. J. van Daal, Abraham Z. Vollan, Shiwei Wang, Marleen Welkenhuysen, Zhiwen Ye, Joshua T. Dudman, Barundeb Dutta, Adam W. Hantman, Kenneth D. Harris, Albert K. Lee, Edvard I. Moser, John OKeefe, Alfonso Renart, Karel Svoboda, Michael Häusser, Sebastian Haesler, Matteo Carandini, and Timothy D. Harris. Neuropixels 2.0: A miniaturized high-density probe for stable, long-term brain recordings. *Science*, 372(6539), April 2021.
[47] Tobias Nöbauer, Yuanlong Zhang, Hyewon Kim, and Alipasha Vaziri. Mesoscale volumetric light-field (mesolf) imaging of neuroactivity across cortical areas at 18 hz. *Nature Methods*, 20(4):600609, February 2023.
[48] Steffen Schneider, Jin Hwa Lee, and Mackenzie Weygandt Mathis. Learnable latent embeddings for joint behavioural and neural analysis. *Nature*, 617(7960):360368, May 2023.
[49] Dániel L. Barabási, Ginestra Bianconi, Ed Bullmore, Mark Burgess, SueYeon Chung, Tina Eliassi-Rad, Dileep George, István A. Kovács, Hernán Makse, Thomas E. Nichols, Christos Papadimitriou, Olaf Sporns, Kim Stachenfeld, Zoltán Toroczkai, Emma K. Towlson, Anthony M. Zador, Hongkui Zeng, Albert-László Barabási, Amy Bernard, and György Buzsáki. Neuroscience needs network science. *The Journal of Neuroscience*, 43(34):59895995, August 2023.
[50] Yuri Lazebnik. Can a biologist fix a radio?or, what i learned while studying apoptosis. *Cancer Cell*, 2(3):179182, September 2002.
[51] Crystal F. Davey, Andrew W. Mathewson, and Cecilia B. Moens. Pcp signaling between migrating neurons and their planar-polarized neuroepithelial environment controls filopodial dynamics and directional migration. *PLOS Genetics*, 12(3):e1005934, March 2016.
[52] Tod R. Thiele, Joseph C. Donovan, and Herwig Baier. Descending control of swim posture by a midbrain nucleus in zebrafish. *Neuron*, 83(3):679–691, August 2014.
[53] Shin-ichi Higashijima, Yoshiki Hotta, and Hitoshi Okamoto. Visualization of cranial motor neurons in live transgenic zebrafish expressing green fluorescent protein under the control of theislet-1promoter/enhancer. *The Journal of Neuroscience*, 20(1):206218, January 2000.
[54] Jason Q Ren, William R McCarthy, Hongwei Zhang, Alan R Adolph, and Lei Li. Behavioral visual responses of wild-type and hypopigmented zebrafish. *Vision Research*, 42(3):293299, February 2002.
[55] Alix M.B. Lacoste, David Schoppik, Drew N. Robson, Martin Haesemeyer, Ruben Portugues, Jennifer M. Li, Owen Randlett, Caroline L. Wee, Florian Engert, and Alexander F. Schier. A convergent and essential interneuron pathway for mauthner-cell-mediated escapes. *Current Biology*, 25(11):15261534, June 2015.
[56] Jeremy N Kay, Karin C Finger-Baier, Tobias Roeser, Wendy Staub, and Herwig Baier. Retinal ganglion cell genesis requires lakritz, a zebrafish atonal homolog. *Neuron*, 30(3):725736, May 2001.
[57] F. Del Bene, C. Wyart, E. Robles, A. Tran, L. Looger, E. K. Scott, E. Y. Isacoff, and H. Baier. Filtering of visual information in the tectum by an identified neural circuit. *Science*, 330(6004):669–673, oct 2010.
[58] Johannes Schindelin, Ignacio Arganda-Carreras, Erwin Frise, Verena Kaynig, Mark Longair, Tobias Pietzsch, Stephan Preibisch, Curtis Rueden, Stephan Saalfeld, Benjamin Schmid, Jean-Yves Tinevez, Daniel James White, Volker Hartenstein, Kevin Eliceiri, Pavel Tomancak, and Albert Cardona. Fiji: an open-source platform for biological-image analysis. *Nature Methods*, 9(7):676682, June 2012.
[59] Eftychios A. Pnevmatikakis and Andrea Giovannucci. Normcorre: An online algorithm for piecewise rigid motion correction of calcium imaging data. *Journal of Neuroscience Methods*, 291:8394, November 2017.
[60] Rodrigo Ibarra-García-Padilla, Aubrey Gaylon Adam Howard, Eileen Willey Singleton, and Rosa Anna Uribe. A protocol for whole-mount immuno-coupled hybridization chain reaction (wichcr) in zebrafish embryos and larvae. *STAR Protocols*, 2(3):100709, September 2021.
[61] Kristen P. DElia, Hanna Hameedy, Dena Goldblatt, Paul Frazel, Mercer Kriese, Yunlu Zhu, Kyla R. Hamling, Koichi Kawakami, Shane A. Liddelow, David Schoppik, and Jeremy S. Dasen. Determinants of motor neuron functional subtypes important for locomotor speed. *Cell Reports*, 42(9):113049, September 2023.
[62] Christopher Clark, Oliver Austen, Ivana Poparic, and Sarah Guthrie. 2-chimaerin regulates a key axon guidance transition during development of the oculomotor projection. *The Journal of Neuroscience*, 33(42):1654016551, October 2013.
[63] Charles B. Kimmel, William W. Ballard, Seth R. Kimmel, Bonnie Ullmann, and Thomas F. Schilling. Stages of embryonic development of the zebrafish. *Developmental Dynamics*, 203(3):253310, July 1995.
[64] Lee A. Fuiman, Kirsten R. Poling, and Dennis M. Higgs. Quantifying developmental progress for comparative studies of larval fishes. *Copeia*, 1998(3):602, August 1998.
[65] David Austin. Generate stepper-motor profiles in real time. *EE Times-India*, jan 2005.

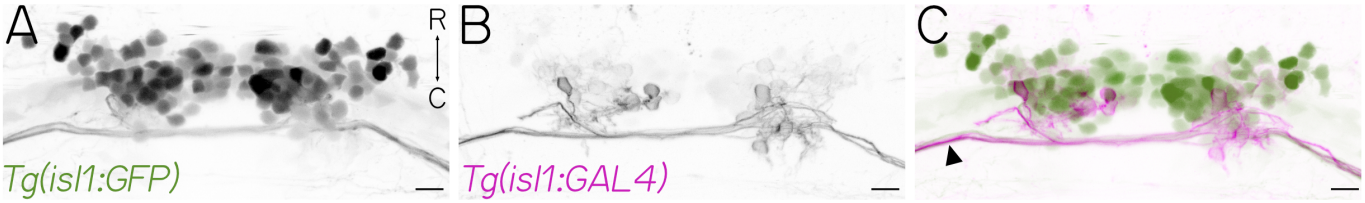

Figure S1: Sparse labeling of superior oblique extraocular motor neurons.
(A-C) Dorso-ventral maximum intensity projection of the extraocular motor neurons of cranial nuclei nIII and nIV visualized in 4 dpf fish using the triple transgenic line *Tg(isl1:GFP)* (A, green) crossed to *Tg(isl1:GAL4);Tg(UAS:KillerRed)* (B, magenta). Scale bar = 10µm.

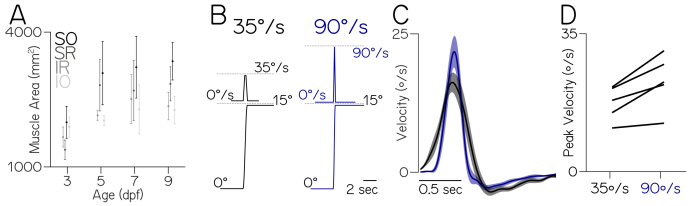

Figure S2: Stronger tilt stimulation evokes faster eye rotations before gaze stabilization behavior is fully mature
(A) Mean area (mm^2) ± SD in all four extraocular muscles from Figures 4H-I. **(B)** Schematic of our standard (left, black) table-tilt stimulus and a faster (right, blue) variant, as described in Figure 1A. Fish are stepped upwards to a a +15° (nose-up) step, held for 7.5 sec, then returned. In black, the peak velocity is 35°/sec and the peak acceleration is 150°/sec. In blue, the peak velocity is 90°/sec and the peak acceleration is 600°/sec. Traces derived from generated stimulus steps. **(C)** Eye velocity traces ± SEM of five fish at 5 dpf stepped using normal (black) or fast (blue) stimuli. **(D)** Mean peak eye velocity of 5 dpf fish for normal (black) and fast (blue) tilts. Peak eye velocities are significantly larger after fast tilts ($p_{t\text{-}test}$ = 0.016, N=5).

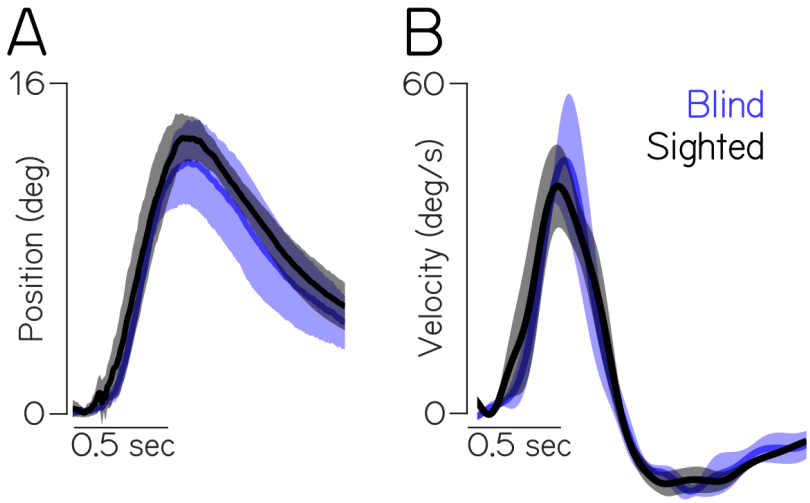

Figure S3: Congenitally blind fish achieve comparable gaze stabilization to sighted siblings
(A) Eye position traces ± SEM of six fish morphologically aged approximately 9 dpf stepped to +15°at peak velocity 35°/sec. Congenitally blind fish traces in blue (n = 3), sighted siblings in black (n = 3). **(B)** Eye velocity traces ± SEM of the same fish in panel A stepped to +15°at peak velocity 35°/sec.